Individual Nanoporous Carbon Spheres with High Nitrogen Content from Polyacrylonitrile Nanoparticles with Sacrificial Protective Layers

Jianan Zhangabet, Rui Yuanat, Sittichai Natesakhawata, Zongyu Wang, Yepin Zhao, Jiajun Yan, Siyuan Liu, Jaejun Lee, Danli Luo, Eric Gottlieb, Tomasz Kowalewski, Michael R. Bockstaller and Krzysztof Matyjaszewski.

^aDepartment of Chemistry, Carnegie Mellon University, 4400 Fifth Ave., Pittsburgh,
Pennsylvania 15213, United States

Department of Materials Science and Engineering, Carnegie Mellon University, 5000 Forbes

Ave., Pittsburgh, Pennsylvania 15213, United States

School of Chemistry and Chemical Engineering, Anhui University and Anhui Province Key

Laboratory of Environment-friendly Polymer Materials, Hefei 230601, China

National Energy Technology Laboratory, United States Department of Energy, P. O. Box 10940,
Pittsburgh, Pennsylvania 15236, United States

Department of Chemical and Petroleum Engineering, University of Pittsburgh, Pittsburgh,
Pennsylvania 15261, United States

ABSTRACT:

Functional nanoporous carbon spheres (NPC-S) are important for applications ranging from adsorption, catalysis, separation to energy storage and biomedicine. The development of effective NPC-S materials has been hindered by the fusion of particles during the pyrolytic process that results in agglomerated materials with reduced activity. Herein, we present a process that enables the scalable synthesis of dispersed NPC-S materials by coating sacrificial protective layers around polyacrylonitrile nanoparticles (PAN NPs) to prevent interparticle crosslinking during carbonization. In a first step, PAN NPs are synthesized using a miniemulsion polymerization, followed by grafting of 3-(triethoxysilyl)propyl methacrylate (TESPMA) to form well-defined core-shell structured PAN@PTESPMA nanospheres. The crosslinked PTESPMA brush layer suppresses crosslinking reactions during carbonization. Uniform NPC-S exhibiting diameters of ~100 nm, with relatively high accessible surface area (~424 m²/g), and high nitrogen content (14.8 wt%) was obtained. When compared to regular nanoporous carbon monolith (NPC-M), the nitrogen-doped NPC-S demonstrated better performance for CO₂ capture with a higher CO₂/N₂ selectivity, an increased efficiency in catalytic oxygen reduction reactions as well as improved electrochemical capacitive behavior. This miniemulsion polymerization-based strategy for the preparation of functional PAN NPs provides a new, facile approach to prepare high-performance porous carbon spheres for diverse applications.

KEYWORDS: nanoporous carbon, polyacrylonitrile, carbon, miniemulsion polymerization, coreshell nanoparticle, SI-ATRP

INTRODUCTION

Nanoporous carbons (NPC) are attracting significant scientific and technological interest due to their use in various applications including catalysis, ¹⁻² water and air purification, ³⁻⁴ and energy storage and conversion. ⁵⁻⁶ Various synthetic strategies have been developed to prepare NPC, including direct carbonization of crosslinked/conjugated polymers and metal—organic frameworks (MOFs), ⁷⁻⁸ high-temperature chlorination of carbide materials, ⁹⁻¹⁰ self-assembly of block copolymer templates, ¹¹⁻¹⁷ and hard templated nanoporous silica and zeolites. ¹⁸⁻²⁰

Recently, nanoporous carbon spheres (NPC-S) possessing unique properties of controllable porous structure and spherical morphology find applications in catalysis, adsorption, water and air purification, biomedicine, and energy storage and conversion.²¹ However, such nanoporous carbons are hydrophobic and have a limited number of active sites which impede their broader commercial applications.²² Doping of NPC-S with heteroatoms such as nitrogen, sulfur, oxygen, and fluorine resulted in significantly enhanced surface polarity, electrical conductivity, and electron-donor tendency of the mesoporous carbons.²³⁻²⁴ This enhanced NPC-S performance in CO₂ capture, electric double-layer capacitors (EDLCs), fuel cells, and catalysis.²⁵⁻²⁶ Further improvements of NPC-S require synthesis of nitrogen-doped NPC-S with both high nanoporosity and unique catalytic properties within the carbon frameworks.

Indeed, over the past decade, there has been explosive growth in the synthesis, characterization, and application of NPC-S materials. Synthetic strategies include templating,²⁷ hydrothermal carbonization (HTC),²⁸⁻²⁹ emulsion polymerization,²⁹ self-assembly,³¹ and modified Stöber methods.²² Due to chain crosslinking and fusion between neighboring nanospheres during high-temperature carbonization, NPC-S materials often agglomerate, diminishing their performance. Thus, synthesis of uniform 'individual' NPC-S presents an outstanding challenge of significant technological relevance.³³

Herein, we demonstrate a novel core/shell particle-based strategy for the preparation of uniform NPC-S with high surface area and high nitrogen content. This method is based on the miniemulsion synthesis of functional polyacrylonitrile (PAN) nanoparticles (NPs) and the subsequent grafting of poly(3-(triethoxysilyl)propyl methacrylate (PTESPMA) from the particles to form PAN@PTESPMA core/shell particles through surface-initiated atom transfer radical polymerization (SI-ATRP). The crosslinked PTESPMA layer acts as a protective shell and sacrificial barrier to avoid fusion of neighboring PAN cores during the carbonization process thereby generating individual NPC-S after removal of the outer shell. The prepared N-doped NPC-S are effective catalysts in multiple applications. The presented easily scalable process forms NPC-S with the desired nanostructure and functionality, as confirmed by enhanced performance in numerous applications.

EXPERIMENTAL SECTION

Chemicals. Acrylonitrile (AN, 99.9%, Acros), divinylbenzene (DVB, 80%, Aldrich), and (3-(triethoxysilyl)propyl methacrylate (TESPMA, Acros) were purified directly before use by passing through a short alumina column to remove the stabilizer. Copper (I) chloride (99.999%, Aldrich) was purified by washing with acetic acid several times followed by filtration, and stored over nitrogen before use. 2,2′ -azobis(2-methylpropionitrile) (AIBN, 98%, Aldrich) was purified by recrystallization from ethanol. Copper (II) chloride (99.999%, Aldrich), 2,2-bipyridine (99%, Aldrich), N,N-dimethylformamide (DMF, Fisher), hexadecane (HD, ≥99%, Aldrich), sodium dodecyl sulfate (SDS, Aldrich), carbon tetrabromide (CBr₁, 99%, Aldrich), and hydrofluoric acid (HF, 50 wt%, Acros) were used as received.

Synthesis of functional PAN NPs by miniemulsion polymerization. Crosslinked PAN NPs were prepared via miniemulsion polymerization at 65 °C. In a typical synthesis, 0.8 g of HD and

0.3 g of AIBN were first added to a mixture of 15.0 g of AN and 1.8 g of DVB to form an oil phase. A portion of SDS aqueous solution was employed as the water phase. The mixture of oil phase and water phase was first pre-emulsified by mechanical stirring for 0.5 h and then the miniemulsion was prepared by sonication for 10 min in an ice bath and the polymerization was carried out at 65 °C in a 250-ml four—neck round bottom flask equipped with a reflux condenser and an agitator. After 30 min of polymerization, when the conversion was nearly 70%, a CBr₄ solution (0.01 g of CBr₄ in 1.0 g of monomer) was added to the ongoing miniemulsion polymerization. The polymerization was allowed to proceed for 8 h under N₂ atmosphere to obtain the crosslinked PAN NPs with accessible ATRP initiating sites on each particle. The yields of PAN NPs were determined to be 91 wt% by gravimetric analysis. The colloids were purified with MeOH and DI water to remove impurities by centrifugal technique before drying under vacuum.

Preparation of PAN NPs with PTESPMA brushes by grafting via SI-ATRP. A suspension of the obtained PAN NPs (0.8 g) in 40 mL of anisole was mixed in a 100 mL dry flask with a stirring bar. After ultrasonication for 30 min and degassing with nitrogen for 30 min under stirring, TESPMA (8.0 g, 80 mmol), CuBr (0.0573 g, 0.4 mmol), and bpy (0.1248 g, 0.8 mmol) were added to the flask. Subsequently, the solution was frozen, and three freeze-pump-thaw cycles were performed to remove oxygen. Polymerization was then carried out at 60 °C under vigorous stirring for 24 h. The final product was recovered by precipitation in methanol. The obtained crosslinked PAN NPs with surface tethered PTESPMA brushes were rinsed with THF by repeated sequential centrifugation and then resuspended in THF. The monomer conversion was determined by gravimetric measurement.

Preparation of N-doped NPC-S from PAN-g-PTESPMA brushes. The overall synthetic procedure is shown in Scheme 1. In a typical synthesis, a certain amount of crosslinked PAN NP-

g-PTESPMA brushes was added to 10 mL of an aqueous ZnCl₂ solution, and the concentration of ZnCl₂ in the aqueous solution was adjusted to 60 wt% by adding water. The mixture was stirred for 24 h at room temperature and then the resulted PAN/silica solution was freeze-dried to obtain solid PAN/silica core/shell composite NPs. The composite was carbonized at 700 °C for 3 h under nitrogen to yield a silica—carbon particles followed by stirring in 50 wt% aqueous HF solution for 12 h to generate individual N-doped nanoporous carbon spheres (NPC-S) after complete removal of the silica shell. For comparison, nanoporous carbon monolith (NPC-M) was obtained under the same procedure using pure PAN NPs as the precursor.

Characterization. The resulting nanocarbon materials were studied by transmission electron microscopy (TEM) operating at 200 kV. Nitrogen adsorption isotherms were measured in a Micromeritics ASAP 2010 volumetric gas adsorption analyzer. X-ray diffraction (XRD) patterns were recorded on a Rigaku Geigerflex equipped with a theta/theta goniometer. The Raman spectra were collected using a Jobin Yvon T64000 triple Raman system (ISA, Edison, NJ) in a subtractive mode with microprobe sampling optics. The excitation was at 514.5 nm (Art laser, Model 95, Lexel Laser, Fremont, CA). X-ray photoelectron spectroscopy (XPS) was performed using an ESCALAB 250Xi X-ray photoelectron spectrometer microprobe, with a 900 μm spot size.

Gas sorption measurements. Sorption isotherms of CO₂ and N₂ were collected using a Quantachrome Autosorb 1-C. Prior to measurements, samples were degassed at 300 °C under vacuum overnight. Brunauer–Emmett–Teller (BET) surface areas were determined from N₂ adsorption isotherms at 77 K. Multipoint BET measurements were performed at relative pressures (P/P₀) in the range of 0.05-0.2 CO₂ and N₂ adsorption isotherms were conducted in the temperature and pressure ranges of 0-50 °C (only 25 °C for N₂) and 0-760 Torr, respectively. The pore size

distribution (PSD) was obtained from Barett-Joyner-Halenda (BJH) method from the adsorption branch.

Electrochemical measurements. A glassy carbon (GC) electrode (5 mm, from Gamry) was carefully polished with 3 μm, 1 μm, and 0.25 μm diamond successively to obtain a mirror-like surface. The electrode was then washed with double-distilled water and acetone and finally dried in air. Five milligrams of the selected carbon material were dispersed in 1 mL of a solvent mixture of Nafion (5%) and ethanol (1/9, v/v) by sonication for 1 h. Twenty microliters of the solution were drop-cast on the GC electrode surface and dried in air to obtain the catalyst loading of 0.5 mg/cm². Voltammograms were recorded at 25 °C with a Gamry Reference 600 potentiostat. Measurements were carried out at a scan rate of 10 mV/s or 100 mV/s using the nanocarbon-modified GC disk as working electrode and a graphite rod counter electrode in Ar-saturated or O₂-saturated 0.1 M aqueous KOH electrolyte. Potentials were recorded versus an Ag/AgCl reference electrode. All potentials were converted to reversible hydrogen electrode (RHE) according to the equation: E _(100,000,000) = E_(100,000,000) + E_(100,000,000) + O₂(100,000) × pH.

Kinetics of the oxygen reduction reaction (ORR) process was followed by Koutecky-Levich analysis of linear sweep voltammograms using Koutecky-Levich equations:

$$\frac{1}{j} = \frac{1}{j_L} + \frac{1}{j_K} = \frac{1}{B\omega^{1/2}} + \frac{1}{j_K}$$

$$B = 0.62n_e F C_0 D_0^{2/3} v^{-1/6}$$

$$j_K = n_e F k C_0$$

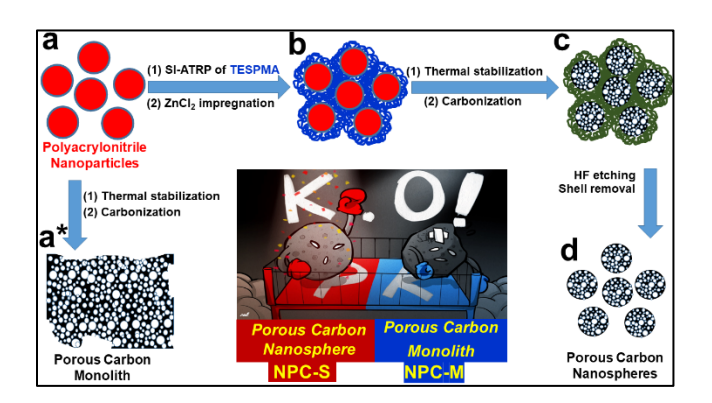
where j (mA/cm²) is the measured current density, j_{κ} and j_{L} (mA/cm²) are the kinetic- and diffusion-limiting current densities, ω is the angular velocity of the rotating disk ($\omega = 2\pi N$, where N is the linear rotating speed in rpm), ne is the overall number of electrons transferred in ORR, F is the Faraday constant (96485 C/mol), C_0 is the bulk concentration of O_2 (1.2 × 10³ mol/L), D_0 is

diffusion coefficient of O_2 (1.9 × 10⁻⁵ cm²/s), ν is the kinematic viscosity of the electrolyte (0.01 cm²/s), and k is the electron transfer rate constant, respectively. The number of electrons transferred (n_e) and the kinetic-limiting current j_k can be obtained from the slope and intercept of the Koutecky–Levich plots (1/j versus $\omega^{-1/2}$), respectively.

Fabrication of supercapacitor devices. Electrochemical measurements were carried out on a potentiostat (Biologic SP-300) in a two-electrode system with 1 M aqueous Na,SO, electrolyte. Electrochemical cells were prepared using a Teflon Swagelok with porous polyolefin separator (Celgard Inc.). The cyclic voltammetry (CV) curves were obtained at various scan rates from 2 to 2000 mV/s in the range of 0 to 0.8 V. Galvanostatic charge-discharge (GCD) curves were obtained at various current densities from 0.1 to 20 A/g. Electrochemical impedance spectroscopy (EIS) measurements were performed in the frequency range of 0.1 Hz to 800 kHz with sinusoidal signal of 5 mV. The electrodes were fabricated by mixing the 70 wt% of NPC-S, 15 wt% acetylene black as a conductive additive and 15 wt% of poly(vinylidene fluoride) as a binder. The mixture was homogenized in NMP by sonication for 10 min and the slurry was deposited on a nickel foam with a diameter of 13 mm and dried in a 100 °C vacuum oven for 24 h.

RESULTS AND DISCUSSION

1. Formation of N-doped NPC-S templated from PAN NP brushes



Scheme 1. Schematic illustration of the process to synthesize NPC-S and NPC-M. (a) Formation of PAN NPs by miniemulsion polymerization, (b) Preparation of PAN NP-g-PTESPMA brushes from PAN NP cores by SI-ATRP, (c) ZnCl₂ impregnation, thermal stabilization, and carbonization of PAN@PTESPMA under a nitrogen atmosphere to stabilize the structure of the nanostructured carbon/silica hybrids, (d) HF etching to generate NPC-S, and (a*) Preparation of NPC-M by direct carbonization of PAN NPs without protective shell.

Scheme 1 illustrates the simple synthetic route developed to fabricate NPC-S starting from PAN NP precursor. The PAN NPs were prepared by miniemulsion polymerization followed by the surface chemistry mediated by a late addition of a CBr₄ chain transfer agent to introduce at the surface of NP, a high concentration of alkyl bromides as ATRP initiators (Scheme 1a). Subsequent SI-ATRP grafting of poly(3-(triethoxysilyl)propyl methacrylate (PTESPMA) yielded PAN particles with surface tethered brushes of cross-linkable PTESPMA chains. A core/shell structured PAN@PTESPMA was subsequently obtained after shell crosslinking under basic conditions (Scheme 1b). Porous carbon/silica hybrids were obtained by ZnCl₂ impregnation of the core, followed by thermal stabilization and carbonization (Scheme 1c). The thermal stabilization process was carried out under air and carbonization of stabilized PAN nanodomains, which concomitantly evaporate ZnCl₂, was performed under an inert atmosphere. The crosslinked PTESPMA shell provided a layer of organosilica that prevented fusion of PAN NP cores during the carbonization procedure, thus generating individual NPC-S after removal of outer silica shell (Scheme 1d). However, without protective shell, NPC-M was obtained by direct carbonization of PAN NPs (Scheme 1a*).

2. Morphology of PAN NPs and NPC-S

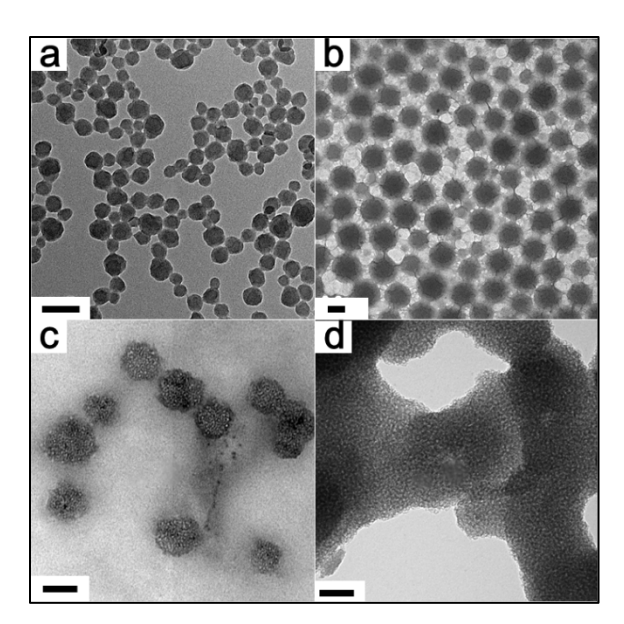


Figure 1. TEM images of (a) crosslinked PAN NPs, (b) core-shell structured PAN@PTESPMA nanospheres prepared by SI-ATRP, (c) NPC-S templated from PAN@PTESPMA nanospheres after the removal of protective shell, and (d) NPC-M prepared from crosslinked PAN NPs without the grafted PTESPMA. Scale bars are 100 nm in all figures.

Transmission electron microscopy (TEM) images of PAN NPs, core-shell structured PAN@PTESPMA nanospheres, NPC-S templated from PAN@PTESPMA nanospheres, and NPC-M prepared from crosslinked PAN NPs without the grafted PTESPMA are shown in Figure 1. Bromo-initiators for ATRP were immobilized on the surfaces of crosslinked PAN NPs by miniemulsion polymerization using CBr₄ as the chain transfer agent.³⁷ The as-prepared PAN NPs had quite a uniform size with a diameter < 100 nm (Figure 1a). After grafting from the surface of the PAN NPs, core-shell structured PAN@PTESPMA nanospheres were obtained and the average size of the NPs increased to ~170 nm (Figure 1b). A two-step thermal treatment of the prepared PAN@PTESPMA nanoparticles was employed to form N-doped NPC-S, as previously used to produce PAN-derived porous nanocarbons.^{16,18} The stabilization of PAN core was achieved by heating the particles at 280 °C for 1 h under air, which resulted in partial crosslinking and

cyclization of PAN side chains. Subsequent carbonization at 700 °C for 2 h under a nitrogen atmosphere did retain nanostructure stabilized during the previous step.* N-doped NPC-S were obtained after etching of the protective silica shell. Figure 1c shows images of the NPC-S revealing that the crosslinked PTESPMA shell was successfully removed to generate the desired individual carbon spheres. For comparison, PAN NPs without the grafted PTESPMA shell were also carbonized and instead of carbon spheres, NPC monoliths was obtained due to the aggregation and fusion of solid PAN NPs during the carbonization process, nevertheless, the derived carbon did retain a highly porous structure (Figure 1d). Therefore, the formation of NPC-S was mainly enabled by the cooperative formation of a crosslinked PTESPMA shell on the surface of PAN core templates.

3. Structural and chemical identity of NPC-S

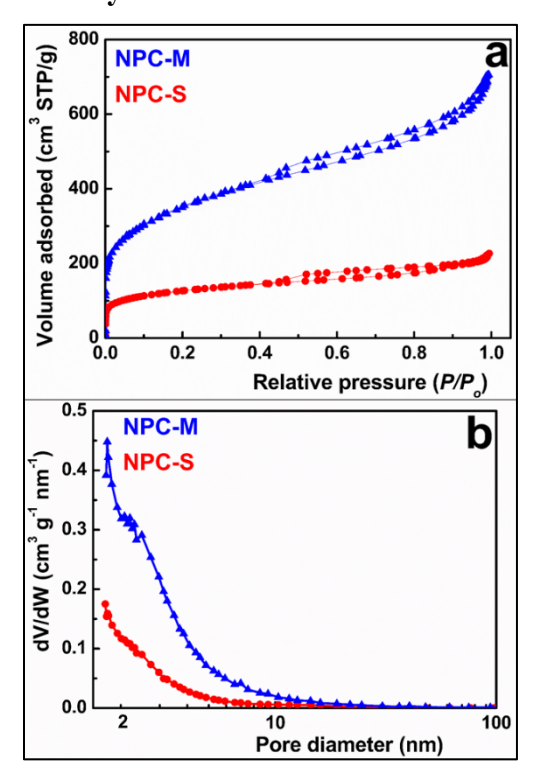


Figure 2. (a) N₂ adsorption and desorption isotherms and (b) the pore size distribution of the asprepared NPC-S and NPC-M.

Brunauer–Emmett–Teller (BET) surface area (S_{BET}) was determined from N₂ adsorption isotherms at 77 K. As displayed in Figure 2a, nitrogen sorption isotherms of the as-prepared porous carbons showed a hysteresis loop, indicating the existence of mesopores. The specific surface area (SSA) of NPC-S was ~424 m²/g. However, the total SSA of NPC-M, formed without the protective shell of PTESPMA, increased up to about 1212 m²/g after the impregnation of ZnCl₂. During pyrolysis, the presence of ZnCl₂ not only promoted the carbonization process of PAN but enhanced mesopore generation after the evaporation of ZnCl₂.³⁹ The SSA of NPC-M was much higher than that of NPC-S mainly because the protective shell of crosslinked PTESPMA impeded the penetration of ZnCl₂ to the core of PAN@PTESPMA nanospheres whereas the full impregnation of ZnCl₂ enhanced the formation of highly porous structure of the aggregated NPC-M. The pore size distributions calculated using the Barrett-Joyner-Halenda (BJH) model show that the majority of the pores fall in the range of 2–10 nm for both NPC-S and NPC-M (Figure 2b). For comparison, without the addition of ZnCl₂, the SSA of pure PAN homopolymer derived porous carbon (NPC-P) was only 191 m²/g with a narrower pore size range, mainly below 3 nm (Figure S1), which confirmed the dehydration effect and activation role ZnCl₂ played a key in the formation of the highly porous microstructure during the carbonization process. XPS confirmed that the residual zinc content in NPC-S was negligible, 0.0054 wt%, which means that the salt essentially evaporated during the carbonization process.

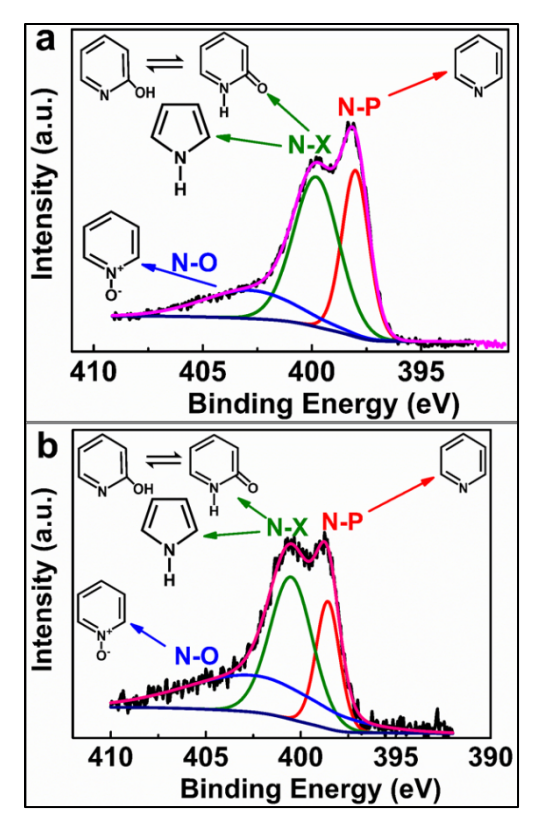


Figure 3. XPS N 1s spectra of the as-prepared NPC-S (a) and NPC-M (b).

The nitrogen content of NPC-S and NPC-M were assessed by elemental analysis (combustion method), which showed contents of 14.8 wt% and 6.1 wt% respectively, indicating that under the selected pyrolysis conditions the PAN precursor yielded nanoporous carbons with high nitrogen content. The type of nitrogen species and the surface elemental composition of nanoporous carbons were evaluated by X-ray photoelectron spectroscopic (XPS) analysis. Survey spectra of the samples found the surfaces to be dominated by carbon, nitrogen, and oxygen as expected (Figure S2). The surface N contents of NPC-S and NPC-M were 14.0 wt% and 5.7 wt% respectively, which are comparable with the results of elemental analysis. The consistency between elemental analysis and XPS is indicative of nitrogen content being uniformly distributed throughout the bulk of the nanoporous carbon structure (Table S1). As shown in Figure 3, the nitrogen atoms of NPC-S and NPC-M were chemically identified. The N 1s spectra of NPC-S and NPC-M were

deconvoluted to form three peaks which were attributed to pyridinic-N (N-P), pyrrolic-/pyridonic-N (N-X), and pyridine oxide (N-O), respectively. The three peaks of NPC-S included N-P (398.9 eV), N-X (400.7 eV), and N-O (403.5 eV) indicating the presence of N-P (33.0%), N-X (46.5%), and N-O (20.5%), respectively. Comparatively, the three peaks of NPC-M yielded N-P (398.6 eV, 21.5%), N-X (400.5 eV, 43.2%), and N-O (402.5 eV, 35.3%), respectively. By comparing the calculated surface molar ratio of these peaks, the main difference between NPC-S and NPC-M was the quantitative content of N-P in the carbon frameworks yielding a fraction of N-P in NPC-S and NPC-M of 33.0% and 21.5%, respectively (Table S2). The pyridinic nitrogen (N-P) are bonded to two C atoms in six-membered rings at the edge of the graphitic carbon layer, which provides the predominant initial active sites for electrochemical behavior.⁶⁻⁴¹ In particular, the presence of N-P sites has been shown to be essential for the ORR.⁶¹ Therefore, the much higher yield of N-P in NPC-S will account for the enhanced comprehensive performance, which is discussed in the following sections.

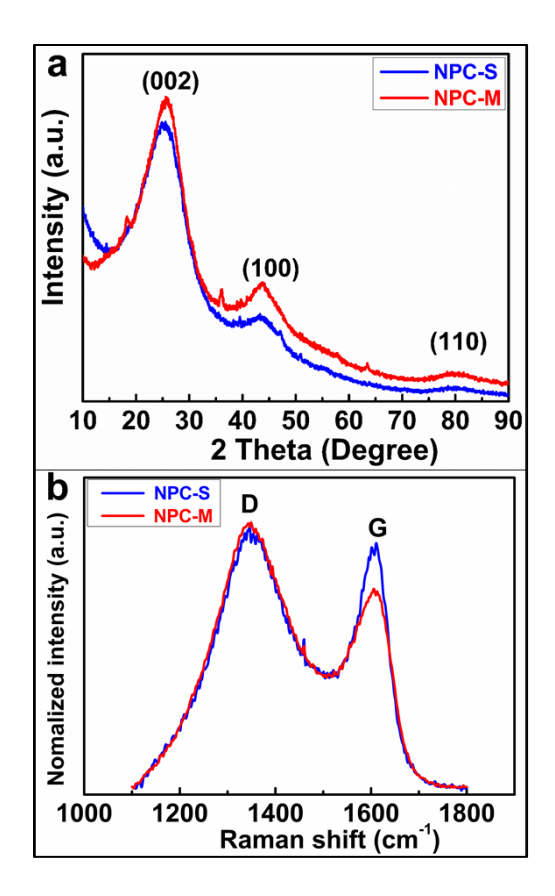


Figure 4. XRD profiles (a) and Raman scattering spectra (b) of the as-prepared NPC-S. The curves were shifted vertically for a clear comparison.

XRD patterns for the NPC-S and NPC-M are shown in Figure 4a. The observed broad Bragg peaks at 2 θ of 25°, 45°, and 80° can be identified as the (002), (101), and (110) reflections of a partially graphitic structure, commonly observed in pyrolytic carbons. Raman spectroscopy provided further information on the surface and topology of the porous carbon materials. As shown in Figure 4b, the typical Raman spectra of NPC-S and NPC-M exhibited D bands at about 1349 cm² with nearly the same bandwidth (<3% difference) and G bands located at 1610 and 1615 cm², respectively. The G band corresponds to the sp² carbon-bonded graphitic structure, which is beneficial for enhancing the electrical conductivity of carbon materials. The peaks G band were further decomposed into 2 Lorentzians for the D/G bands and a Gaussian, which is generally attributed to amorphous graphitic phase. The bandwidth of the G band was 21% narrower in the

NPC-S compared to the NPC-M indicating larger graphitic domains (Figure S3). Furthermore, the integrated D/G ratio is generally proportional to the degree of graphitization, which are 4.3 and 4.6 for NPC-S and NPC-M, respectively.⁴³⁻⁴⁴ The lower integrated D/G ratio of NPC-S indicates that the sample has a higher degree of graphitization and thereby should exhibit the better electronic conductivity, which is desirable for use as electrode materials for energy storage devices.

4. CO₂ capture performance of NPC-S

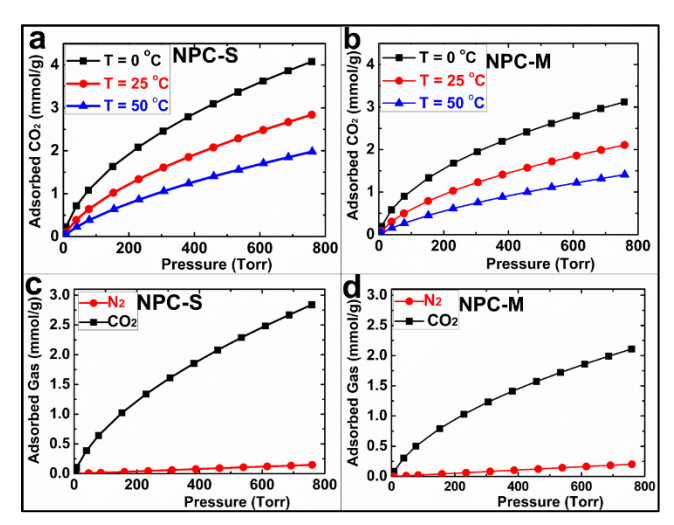


Figure 5. CO₂ adsorption isotherms at different temperatures for NPC-S (a) and NPC-M (b). CO₂ and N₂ adsorption isotherms at 298 K for NPC-S (c) and for NPC-M (d).

The capture of CO₂ has attracted considerable attention in recent years because it is the main anthropogenic contributor to climate change.⁴⁵ Various porous solids including zeolites, metalorganic frameworks (MOFs), covalent organic frameworks, polymers, and nanocarbons, have been investigated for CO₂ capture.⁴⁶⁻⁵⁰ Among them, porous carbons have attracted intense interest due to the relatively low cost, simple fabrication, and high thermal stability of carbon.⁵¹⁻⁵² The adsorption properties of porous carbon are dependent on the pore structures and surface properties, including nitrogen content. As shown in Figure 5a, the CO₂ sorption isotherms of N-doped NPC-S showed high CO₂ capacities of 4.1, 2.8, and 2.0 mmol/g at 273, 298, and 323 K, respectively.

Comparatively, as shown in Figure 5b, the CO₂ sorption isotherms of N-doped NPC-M demonstrated much lower performance for CO₂ capture with the adsorption capacity of only 2.1 mmol/g at 298 K and 760 Torr, despite that NPC-M had a much higher SSA of 1212 m²/g. We interpret this surprising result as a consequence of higher nitrogen content of NPC-S. Nitrogen atoms should act as Lewis basic sites for anchoring acidic CO₂ molecule thus increasing the CO₂ adsorption capacity. This implies that the higher nitrogen content, 14.8 wt% in the NPC-S materials as compared to 6.1 wt% for NPC-M, generated more exposed basic sites which resulted in the enhanced interactions between N-containing functional groups and CO₃, and thus significantly improved the CO₂ adsorption capacity. Therefore, the high nitrogen content played a more decisive role in the performance of CO₃ capture than the higher SSA of porous carbons. Note that, no saturation is observed up to a pressure of 760 Torr, suggesting that higher CO₃ adsorption capacity can be achieved at a higher pressure.

Moreover, the CO₂/N₂ selectivity of NPC-S and NPC-M, calculated as a molar ratio of CO₂ and N₂ adsorbed at 760 Torr, turned out to be 19.12 and 10.46, respectively, as shown in Figure 5c and 5d. NPC-S exhibited better selectivity for CO₂ capture manifested by the ~20:1 ratio of adsorbed CO₂ over N₂, which is a result of its higher nitrogen content.⁵⁵ The initial slopes of the CO₂ and N₂ adsorption isotherms of NPC-S were calculated to be 11.15 and 0.42, respectively. Therefore, the ratio of initial slopes is as high as 27:1, indicating that the NPC-S has a high selectivity in adsorbing CO₂ in a CO₂/N₂ mixed gas.²⁵

Previous reports have shown performance of commercial activated carbon, carbon molecular sieves, and cobalt adeninate bio-MOFs with capacities of up to 2.1, 4.5, and 6.0 mmol/g at 273 K, respectively. Comparing these results to NPC-S, it is clear that the prepared PAN-derived porous carbon spheres provide a high adsorption capacity and selectivity for CO₂ capture. It is well known

that KOH or CO₂ activation provides a large volume of fine micropores (~0.5 cm³/g) in the carbons which is beneficial for CO₂ sorption.^{52,61} However even without further KOH or CO₂ activation, the relatively high CO₂ adsorption of our as-prepared NPC-S demonstrated that the high nitrogendoping level of NPC-S effectively enhanced CO₂ adsorption at ambient conditions.⁶²

5. NPC-S as electrocatalysts for ORR and supercapacitors

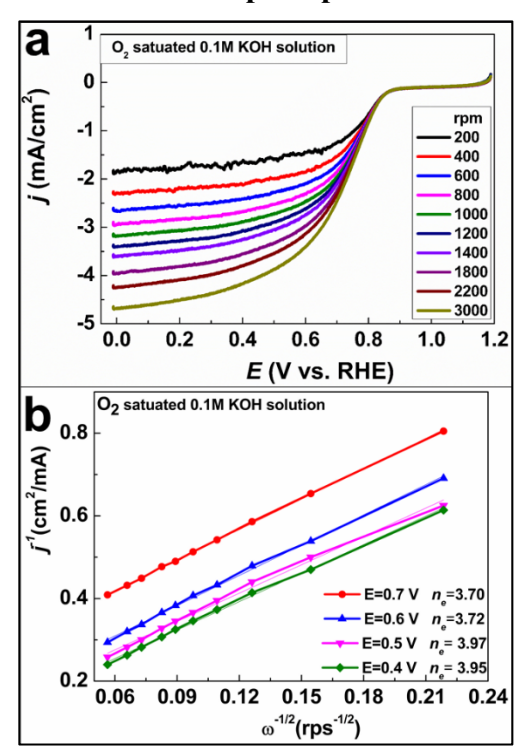


Figure 6. Electrochemical characterization of NPC-S as an electrocatalyst for ORR. (a) Rotating disk electrode study in O₂-saturated 0.1 M KOH electrolyte at a scan rate 10 mV/s and (b) Koutecky-Levich analysis of LSV curves presented in (a).

The presence of nitrogen in formed NPC-S could significantly enhance the performance of the carbons as electrodes for supercapacitors and catalysts for oxygen reduction reaction (ORR).^{15,55} To demonstrate such an improvement a sample of the NPC-S powder was dispersed in an ethanol solution containing Nafion as a binder and then deposited on a polished glassy carbon (GC) working electrode. The electrocatalytic activity of NPC-S was further investigated by cyclic

voltammetry (CV) measurements in 0.1 M KOH solution at room temperature. Compared to CV curves obtained under saturated Ar, a pronounced reduction peak appeared in the system continuously purged with oxygen (Figure S4), pointing to good ORR performance. Linear sweep voltammograms (LSV) were then recorded using a rotating disk electrode (RDE) to evaluate the ORR kinetics of NPC-S electrodes. As shown from the polarization curves in Figure 6a, current density increased with increasing rates of rotation. The onset overpotential of NPC-S based electrode was observed to be ~0.87 V vs RHE. Koutecky–Levich (K-L) analysis was further performed to calculate the number of transferred electrons (n.) (Figure 6b). The linear relationship between the current density (j-1) and square root of the rotation speed (ω-12) was observed in a large potential range (0.4-0.7 V vs RHE). n_c was determined to be 3.85 ± 0.12 by the K-L equations, which meant the reaction proceeds as an efficient four-electron transfer process for NPC-S materials. Therefore the nitrogen-doped NPC-S materials can be used as efficient electrocatalysts in ORR in the presence of an alkaline electrolyte.

In comparison, the n, of NPC-M based electrode was in the range of 5.13 and 5.68 (Figure S5), which indicated that side reactions took place in the oxygen reduction process. From all nitrogen species present in a carbon electrode, the pyridinic nitrogen, with the lone pair residing on the sp² orbital, should be the most electrochemically active. The ratios of peak area from XPS of pyridinic nitrogen are 21.5 and 33% for NPC-M and NPC-S, respectively (Table S2). Therefore, the incorporation of nitrogen atoms with a higher fraction of pyridinic nitrogen into a carbon framework has a significant influence over the resulting ORR performance. Furthermore, compared with NPC-M, a lower mass transport and charge transfer resistance of the spherical characteristics in NPC-S may contribute to the improved electrocatalytic activity for ORR.

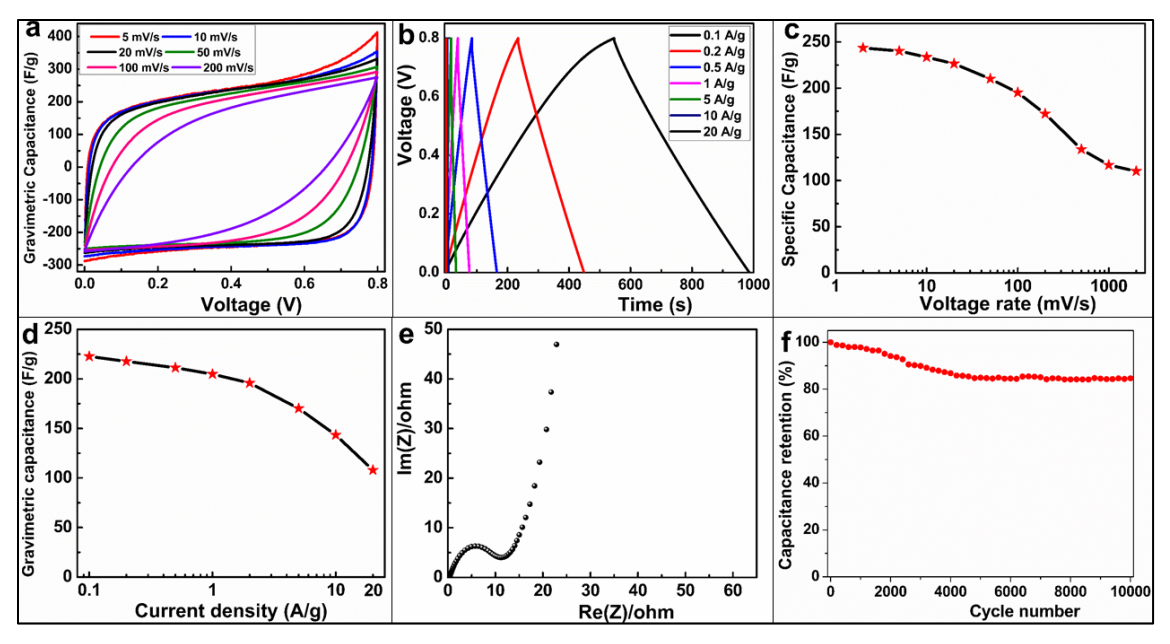


Figure 7. Electrochemical capacitive behavior of NPC-S measured in a two-electrode system by using 1 M Na₂SO₄ aqueous solution as electrolyte within the potential range of 0 to 0.8 V. (a) cyclic voltammetry (CV) curves at various scan rates, (b) galvanostatic charge-discharge curves at different current densities, (c) specific capacitance as a function of scan rate ranging from 2 to 2000 mV/s, (d) specific capacitance as a function of current density ranging from 0.1 to 20 A/g, (e) the Nyquist plot, and (f) cycle durability at a current load of 2 A/g.

Figure 7a shows the representative cyclic voltammetry (CV) curves obtained at scan rates in the range of 5, 10, 20, 50, 100, and 200 mV/s. The curves exhibited a rectangular shape without the presence of redox peaks, demonstrating ideal supercapacitive performance with a fast charging-discharging process. Particularly noteworthy is the observation that the CV curve obtained at the highest scan rate of 200 mV/s almost retained the initial rectangular shape measured at 5 mV/s, indicating good electrochemical rate performance. Figure 7b shows the galvanostatic charge/discharge (GCD) curves of the device at various current densities ranging from 0.1 to 2 A/g. All charge-discharge curves were linear and symmetrical with a gradual slope change at various current densities. This is the typical characteristic of an ideal capacitive performance,

which was also consistent with the CV results. The typical triangular profiles confirmed good electrochemical capacitive properties with a specific capacitance of ~244 F/g at a current density of 100 mA/g, which was much higher than the supercapacitor based on NPC-M (~175 F/g) under the same conditions (Figure S6). Figure 7c and 7d show the dependence of gravimetric capacitance on the scan rate and current density. It is noteworthy that with high charge/discharge rate, the specific capacitance was generally maintained (45% from 2 to 2000 mV/s, 49% from 0.1 to 20 A/g). This outstanding rate performance was attributed to low internal resistance and highly porous structure of NPC-S. To further analyze charge transport and ion diffusion of NPC-S, electrochemical impedance spectroscopy (EIS) was used in electrochemical tests. In Figure 7e, the x-intercept of the Nyquist plots represents the equivalent series resistance (ESR) of 0.3 Ω and semicircle show an internal resistance of 11.8 Ω . The low resistance illustrated an ideal performance as supercapacitor electrodes. In low-frequency region, the nearly vertical slope of the Nyquist plots demonstrated good ion diffusion in the electrolyte to the electrode. Figure 7f shows the recycling stability of NPC-S by galvanostatic charge/discharge at a current density of 2 A/g for 10000 cycles. The capacitance became stable with about 85% retention of performance, thereby exhibiting excellent stability during galvanostatic charge-discharge cycling. The comprehensive properties of these characteristics of NPC-S based supercapacitors are very competitive to other previously reported studies, which makes them very promising electrode materials for highperformance supercapacitors (Table S3).

The carbon nanoparticle synthesis strategy demonstrated in this work is based on the preparation of PAN with PTESPMA brushes allowing the formation of individual NPC-S. Despite the numerous templating methods reported in the literature, this is the first demonstration of controllable fabrication of NPC-S with high surface area and high nitrogen doping using PAN as

a carbon precursor. Such high value of capacitance in NPC-S confirms the contribution of the abundant nitrogen heteroatoms. Compared with conventionally activated carbons (e.g. NPC-M), a much higher N content of NPC-S improved its surface wettability and the spherical shape of NPC-S provided an easily available electrode/electrolyte interface for forming an electric double layer. Therefore, NPC-S based supercapacitors demonstrated an improved EDLC performance due to a lower diffusive limitation. ⁶⁶⁻⁶⁷

CONCLUSION

We have demonstrated a facile, effective, and scalable method to synthesize nitrogen-doped NPC-S, involving the formation of PAN@PTESPMA nanoparticles by SI-ATRP from PAN NPs, carbonization, and subsequent etching process to remove PTESPMA shell. A key feature of this new method for the preparation of individual NPC-S is the presence of a protective PTESPMA shell, which prevents PAN core aggregation/fusion during the carbonization process. Due to the high nitrogen loading of 14.8 wt%, large void space, and high permeability of porous structure spheres, the obtained NPC-S materials exhibited a good performance for CO₂ capture with a high selectivity. The NPC-S are effective catalysts in ORR via a four-electron mechanism and act as high-performance supercapacitors. The significant increase in the performance of electrocatalytic and CO₂-adsorption performance of NPC-S, in conjunction with the economic viability of miniemulsion, make the presented method a promising alternative for the viable development of carbon nanomaterial-based technologies.

ASSOCIATED CONTENT

Supporting Information.

Experimental details and characterization results from BET, XPS, ORR, electrochemical

capacitive behavior (PDF). This material is available free of charge via the Internet at

http://pubs.acs.org.

AUTHOR INFORMATION

Corresponding Author

*bockstaller@cmu.edu

*km3b@anrew.cmu.edu

ORCID

Michael R. Bockstaller: 0000-0001-9046-9539

Krzysztof Matyjaszewski: 0000-0003-1960-3402

Author Contributions

The manuscript was written through contributions of all authors. All authors have given approval

to the final version of the manuscript. ‡These authors contributed equally.

Notes

The authors declare no competing financial interests.

ACKNOWLEDGMENTS

The authors acknowledge funding by the National Science Foundation via grant CMMI-1663305

as well DMR 1501324. The authors further acknowledge financial support by the Wilton E. Scott

Institute for Energy Innovation at Carnegie Mellon University. J.Z. acknowledges a scholarship

23

from the China Scholarship Council (CSC). The authors thank Joel Gillespie of the University of

Pittsburgh Materials Characterization Laboratory (MCL) for access to the XPS spectrometer.

REFERENCES

- (1) Dai, L.; Xue, Y.; Qu, L.; Choi, H.-J.; Baek, J.-B. Metal-Free Catalysts for Oxygen Reduction Reaction. *Chem. Rev.* **2015**, *115* (11), 4823-4892.
- (2) Zhao, Y.; Nakamura, R.; Kamiya, K.; Nakanishi, S.; Hashimoto, K. Nitrogen-Doped Carbon Nanomaterials as Non-Metal Electrocatalysts for Water Oxidation. *Nat. Commun.* **2012**, *4*, 2390.
- (3) Marias, F.; Letellier, S.; Cezac, P.; Serin, J. P. Efficient and Durable Visible Light Photocatalytic Performance of Porous Carbon Nitride Nanosheets for Air Purification. *Ind. Eng. Chem. Res.* **2014**, *53* (6), 2318–2330.
- (4) Gupta, V. K.; Saleh, T. A. Sorption of Pollutants by Porous Carbon, Carbon Nanotubes and Fullerene-an Overview. *Environ. Sci. Pollut. Res.* **2013**, *20* (5), 2828-2843.
- (5) Li, W.; Liu, J.; Zhao, D. Mesoporous Materials for Energy Conversion and Storage Devices. *Nat. Rev. Mater.* **2016**, 1 (6), 16023.
- (6) Roberts, A. D.; Li, X.; Zhang, H. Porous Carbon Spheres and Monoliths: Morphology Control, Pore Size Tuning and Their Applications as Li-lon Battery Anode Materials. *Chem. Soc. Rev.* **2014**, *43* (13), 4341-4356.
- (7) Jiang, H.-L.; Liu, B.; Lan, Y.-Q.; Kuratani, K.; Akita, T.; Shioyama, H.; Zong, F.; Xu, Q. From Metal—Organic Framework to Nanoporous Carbon: Toward a Very High Surface Area and Hydrogen Uptake. *J. Am. Chem. Soc.* **2011**, *133* (31), 11854-11857.
- (8) Chaikittisilp, W.; Ariga, K.; Yamauchi, Y. A New Family of Carbon Materials: Synthesis of Mof-Derived Nanoporous Carbons and Their Promising Applications. *J. Mater. Chem. A* **2013**, *1* (1), 14-19.
- (9) Gogotsi, Y.; Nikitin, A.; Ye, H.; Zhou, W.; Fischer, J. E.; Yi, B.; Foley, H. C.; Barsoum, M. W. Nanoporous Carbide-Derived Carbon with Tunable Pore Size. *Nat. Mater.* **2003**, *2* (9), 591-594.
- (10) Oschatz, M.; Zeiger, M.; Jackel, N.; Strubel, P.; Borchardt, L.; Reinhold, R.; Nickel, W.; Eckert, J.; Presser, V.; Kaskel, S. Emulsion Soft Templating of Carbide-Derived Carbon Nanospheres with Controllable Porosity for Capacitive Electrochemical Energy Storage. *J. Mater. Chem. A* **2015**, *3* (35), 17983-17990.
- (11) Kowalewski, T.; Tsarevsky, N. V.; Matyjaszewski, K. Nanostructured Carbon Arrays from Block Copolymers of Polyacrylonitrile. *J. Am. Chem. Soc.* **2002**, *124* (36), 10632-10633.
- (12) Tang, C.; Tracz, A.; Kruk, M.; Zhang, R.; Smilgies, D.-M.; Matyjaszewski, K.; Kowalewski, T. Long-Range Ordered Thin Films of Block Copolymers Prepared by Zone-Casting and Their Thermal Conversion into Ordered Nanostructured Carbon. *J. Am. Chem. Soc.* **2005**, *127* (19), 6918-6919.
- (13) Kruk, M.; Dufour, B.; Celer, E. B.; Kowalewski, T.; Jaroniec, M.; Matyjaszewski, K. Well-Defined Poly (Ethylene Oxide)-Polyacrylonitrile Diblock Copolymers as Templates for Mesoporous Silicas and Precursors for Mesoporous Carbons. *Chem. Mater.* **2006**, *18* (6), 1417-1424.
- (14) Zhong, M.; Kim, E. K.; McGann, J. P.; Chun, S.-E.; Whitacre, J. F.; Jaroniec, M.; Matyjaszewski, K.; Kowalewski, T. Electrochemically Active Nitrogen-Enriched Nanocarbons with Well-Defined Morphology Synthesized by Pyrolysis of Self-Assembled Block Copolymer. *J. Am. Chem. Soc.* **2012**, *134* (36), 14846-14857.
- (15) McGann, J. P.; Zhong, M.; Kim, E. K.; Natesakhawat, S.; Jaroniec, M.; Whitacre, J. F.; Matyjaszewski, K.; Kowalewski, T. Block Copolymer Templating as a Path to Porous Nanostructured Carbons with Highly Accessible Nitrogens for Enhanced (Electro)Chemical Performance. *Macromol. Chem. Phys.* **2012**, *213* (10-11), 1078-1090.
- (16) Zhong, M.; Jiang, S.; Tang, Y.; Gottlieb, E.; Kim, E. K.; Star, A.; Matyjaszewski, K.; Kowalewski, T. Block Copolymer-Templated Nitrogen-Enriched Nanocarbons with Morphology-Dependent Electrocatalytic Activity for Oxygen Reduction. *Chem. Sci.* **2014**, *5* (8), 3315-3319.
- (17) Ju, M. J.; Choi, I. T.; Zhong, M.; Lim, K.; Ko, J.; Mohin, J.; Lamson, M.; Kowalewski, T.; Matyjaszewski, K.; Kim, H. K. Copolymer-Templated Nitrogen-Enriched Nanocarbons as a Low Charge-Transfer Resistance and Highly Stable Alternative to Platinum Cathodes in Dye-Sensitized Solar Cells. *J. Mater. Chem. A* **2015**, *3* (8), 4413-4419.
- (18) Tang, C.; Bombalskil, L.; Kruk, M.; Jaroniec, M.; Matyjaszewski, K.; Kowalewski, T. Nanoporous Carbon Films from" Hairy" Polyacrylonitrile-Grafted Colloidal Silica Nanoparticles. *Adv. Mater.* **2008**, *20* (8), 1516-1516.
- (19) Yang, X.; Wu, D.; Chen, X.; Fu, R. Nitrogen-Enriched Nanocarbons with a 3-D Continuous Mesopore Structure from Polyacrylonitrile for Supercapacitor Application. *J. Phys. Chem. C* **2010**, *114* (18), 8581-8586.

- (20) Wu, D.; Dong, H.; Pietrasik, J.; Kim, E. K.; Hui, C. M.; Zhong, M.; Jaroniec, M.; Kowalewski, T.; Matyjaszewski, K. Novel Nanoporous Carbons from Well-Defined Poly (Styrene-Co-Acrylonitrile)-Grafted Silica Nanoparticles. *Chem. Mater.* **2011**, *23* (8), 2024-2026.
- (21) Liu, J.; Wickramaratne, N. P.; Qiao, S. Z.; Jaroniec, M. Molecular-Based Design and Emerging Applications of Nanoporous Carbon Spheres. *Nat. Mater.* **2015**, *14* (8), 763-774.
- (22) Wei, J.; Zhou, D.; Sun, Z.; Deng, Y.; Xia, Y.; Zhao, D. A Controllable Synthesis of Rich Nitrogen-Doped Ordered Mesoporous Carbon for Co₂ Capture and Supercapacitors. *Adv. Funct. Mater.* **2013**, *23* (18), 2322-2328.
- (23) Feng, S.; Li, W.; Shi, Q.; Li, Y.; Chen, J.; Ling, Y.; Asiri, A. M.; Zhao, D. Synthesis of Nitrogen-Doped Hollow Carbon Nanospheres for Co₂ Capture. *Chem. Commun.* **2014**, *50* (3), 329-331.
- (24) Liu, S.; Cai, Y.; Zhao, X.; Liang, Y.; Zheng, M.; Hu, H.; Dong, H.; Jiang, S.; Liu, Y.; Xiao, Y. Sulfur-Doped Nanoporous Carbon Spheres with Ultrahigh Specific Surface Area and High Electrochemical Activity for Supercapacitor. *J. Power Sources* **2017**, *360*, 373-382.
- (25) Su, F.; Poh, C. K.; Chen, J. S.; Xu, G.; Wang, D.; Li, Q.; Lin, J.; Lou, X. W. Nitrogen-Containing Microporous Carbon Nanospheres with Improved Capacitive Properties. *Energy Environ. Sci.* **2011**, *4* (3), 717-724.
- (26) Wickramaratne, N. P.; Xu, J.; Wang, M.; Zhu, L.; Dai, L.; Jaroniec, M. Nitrogen Enriched Porous Carbon Spheres: Attractive Materials for Supercapacitor Electrodes and Co₂ Adsorption. *Chem. Mater.* **2014**, *26* (9), 2820-2828.
- (27) Liu, J.; Yang, T.; Wang, D.-W.; Lu, G. Q. M.; Zhao, D.; Qiao, S. Z. A Facile Soft-Template Synthesis of Mesoporous Polymeric and Carbonaceous Nanospheres. *Nat. Commun.* **2013**, *4*, 2798.
- (28) Sun, X.; Li, Y. Colloidal Carbon Spheres and Their Core/Shell Structures with Noble-Metal Nanoparticles. *Angew. Chem. Int. Ed.* **2004**, *43* (5), 597-601.
- (29) Xu, S.; Liu, C.; Ye, F.; Guo, Y.; Wiezorek, J. Alkali-Assisted Hydrothermal Route to Control Submicron-Sized Nanoporous Carbon Spheres with Uniform Distribution. *Colloids Surf. A: Physicochem. Eng. Aspects* **2017,** *515*, 1-11. (30) Ouyang, Y.; Shi, H.; Fu, R.; Wu, D. Highly Monodisperse Microporous Polymeric and Carbonaceous Nanospheres with Multifunctional Properties. *Sci. Rep.* **2013,** *3*, 1430.
- (31) Wang, S.; Li, W.-C.; Hao, G.-P.; Hao, Y.; Sun, Q.; Zhang, X.-Q.; Lu, A.-H. Temperature-Programmed Precise Control over the Sizes of Carbon Nanospheres Based on Benzoxazine Chemistry. *J. Am. Chem. Soc.* **2011**, *133* (39), 15304-15307
- (32) Liu, J.; Qiao, S. Z.; Liu, H.; Chen, J.; Orpe, A.; Zhao, D.; Lu, G. Q. M. Extension of the Stöber Method to the Preparation of Monodisperse Resorcinol–Formaldehyde Resin Polymer and Carbon Spheres. *Angew. Chem. Int. Ed.* **2011**, *50* (26), 5947-5951.
- (33) Gong, K.; Du, F.; Xia, Z.; Durstock, M.; Dai, L. Nitrogen-Doped Carbon Nanotube Arrays with High Electrocatalytic Activity for Oxygen Reduction. *Science* **2009**, *323* (5915), 760-764.
- (34) Ejaz, M.; Ohno, K.; Tsujii, Y.; Fukuda, T. Controlled Grafting of a Well-Defined Glycopolymer on a Solid Surface by Surface-Initiated Atom Transfer Radical Polymerization. *Macromolecules* **2000**, *33* (8), 2870-2874.
- (35) Pyun, J.; Jia, S.; Kowalewski, T.; Patterson, G. D.; Matyjaszewski, K. Synthesis and Characterization of Organic/Inorganic Hybrid Nanoparticles: Kinetics of Surface-Initiated Atom Transfer Radical Polymerization and Morphology of Hybrid Nanoparticle Ultrathin Films. *Macromolecules* **2003**, *36* (14), 5094-5104.
- (36) Hui, C. M.; Pietrasik, J.; Schmitt, M.; Mahoney, C.; Choi, J.; Bockstaller, M. R.; Matyjaszewski, K. Surface-Initiated Polymerization as an Enabling Tool for Multifunctional (Nano-) Engineered Hybrid Materials. *Chem. Mater.* **2013**, *26* (1), 745-762.
- (37) Liu, Y.-Y.; Chen, H.; Ishizu, K. Facile Surface Immobilization of Atrp Initiators on Colloidal Polymers for Grafting Brushes and Application to Colloidal Crystals. *Langmuir* **2011**, *27* (3), 1168-1174.
- (38) Fitzer, E. Pan-Based Carbon Fibers—Present State and Trend of the Technology from the Viewpoint of Possibilities and Limits to Influence and to Control the Fiber Properties by the Process Parameters. *Carbon* **1989**, *27* (5), 621-645.
- (39) Yu, Z. L.; Li, G. C.; Fechler, N.; Yang, N.; Ma, Z. Y.; Wang, X.; Antonietti, M.; Yu, S. H. Polymerization under Hypersaline Conditions: A Robust Route to Phenolic Polymer-Derived Carbon Aerogels. *Angew. Chem.* **2016**, *128* (47), 14843-14847.
- (40) Ding, W.; Wei, Z.; Chen, S.; Qi, X.; Yang, T.; Hu, J.; Wang, D.; Wan, L. J.; Alvi, S. F.; Li, L. Space-Confinement-Induced Synthesis of Pyridinic-and Pyrrolic-Nitrogen-Doped Graphene for the Catalysis of Oxygen Reduction. *Angewandte Chemie International Edition* **2013**, *52* (45), 11755-11759.
- (41) Yang, S.; Feng, X.; Wang, X.; Müllen, K. Graphene-Based Carbon Nitride Nanosheets as Efficient Metal-Free Electrocatalysts for Oxygen Reduction Reactions. *Angew. Chem. Int. Ed.* **2011**, *50* (23), 5339-5343.
- (42) Yu, D.; Zhang, Q.; Dai, L. Highly Efficient Metal-Free Growth of Nitrogen-Doped Single-Walled Carbon Nanotubes

- on Plasma-Etched Substrates for Oxygen Reduction. J. Am. Chem. Soc. 2010, 132 (43), 15127-15129.
- (43) Jawhari, T.; Roid, A.; Casado, J. Raman Spectroscopic Characterization of Some Commercially Available Carbon Black Materials. *Carbon* **1995**, *33* (11), 1561-1565.
- (44) Ferrari, A. C. Raman Spectroscopy of Graphene and Graphite: Disorder, Electron–Phonon Coupling, Doping and Nonadiabatic Effects. *Solid State Commun.* **2007**, *143* (1), 47-57.
- (45) Wang, Q.; Luo, J.; Zhong, Z.; Borgna, A. Co₂ Capture by Solid Adsorbents and Their Applications: Current Status and New Trends. *Energy Environ. Sci.* **2011**, *4* (1), 42-55.
- (46) Sevilla, M.; Fuertes, A. B. Sustainable Porous Carbons with a Superior Performance for Co₂ Capture. *Energy Environ. Sci.* **2011**, *4* (5), 1765-1771.
- (47) Du, N.; Park, H. B.; Robertson, G. P.; Dal-Cin, M. M.; Visser, T.; Scoles, L.; Guiver, M. D. Polymer Nanosieve Membranes for Co₂-Capture Applications. *Nat. Mater.* **2011**, *10* (5), 372.
- (48) Huang, X.; Jiang, P. Core-Shell Structured High-K Polymer Nanocomposites for Energy Storage and Dielectric Applications. *Adv. Mater.* **2015**, *27* (3), 546-554.
- (49) Sumida, K.; Rogow, D. L.; Mason, J. A.; McDonald, T. M.; Bloch, E. D.; Herm, Z. R.; Bae, T.-H.; Long, J. R. Carbon Dioxide Capture in Metal-Organic Frameworks. *Chem. Rev* **2012**, *112* (2), 724-781.
- (50) Banerjee, R.; Phan, A.; Wang, B.; Knobler, C.; Furukawa, H.; O'Keeffe, M.; Yaghi, O. M. High-Throughput Synthesis of Zeolitic Imidazolate Frameworks and Application to Co₂ Capture. *Science* **2008**, *319* (5865), 939-943.
- (51) Tang, J.; Liu, J.; Li, C.; Li, Y.; Tade, M. O.; Dai, S.; Yamauchi, Y. Synthesis of Nitrogen-Doped Mesoporous Carbon Spheres with Extra-Large Pores through Assembly of Diblock Copolymer Micelles. *Angew. Chem. Int. Ed.* **2015**, *54* (2), 588-593.
- (52) To, J. W.; He, J.; Mei, J.; Haghpanah, R.; Chen, Z.; Kurosawa, T.; Chen, S.; Bae, W.-G.; Pan, L.; Tok, J. B.-H. Hierarchical N-Doped Carbon as Co₂ Adsorbent with High Co₂ Selectivity from Rationally Designed Polypyrrole Precursor. *J. Am. Chem. Soc.* **2016**, *138* (3), 1001-1009.
- (53) Rochelle, G. T. Amine Scrubbing for Co₂ Capture. Science 2009, 325 (5948), 1652-1654.
- (54) Xing, W.; Liu, C.; Zhou, Z.; Zhang, L.; Zhou, J.; Zhuo, S.; Yan, Z.; Gao, H.; Wang, G.; Qiao, S. Z. Superior Co₂ Uptake of N-Doped Activated Carbon through Hydrogen-Bonding Interaction. *Energy Environ. Sci.* **2012**, *5* (6), 7323-7327.
- (55) Zhong, M.; Natesakhawat, S.; Baltrus, J. P.; Luebke, D.; Nulwala, H.; Matyjaszewski, K.; Kowalewski, T. Copolymer-Templated Nitrogen-Enriched Porous Nanocarbons for Co₂ Capture. *Chem. Commun.* **2012**, *48* (94), 11516-11518.
- (56) Wang, J.; Senkovska, I.; Oschatz, M.; Lohe, M. R.; Borchardt, L.; Heerwig, A.; Liu, Q.; Kaskel, S. Highly Porous Nitrogen-Doped Polyimine-Based Carbons with Adjustable Microstructures for Co₂ Capture. *J. Mater. Chem. A* **2013**, *1* (36), 10951-10961.
- (57) Tang, Z.; Han, Z.; Yang, G.; Yang, J. Polyethylenimine Loaded Nanoporous Carbon with Ultra-Large Pore Volume for Co₂ Capture. *Appl. Surf. Sci.* **2013**, *277*, 47-52.
- (58) An, J.; Geib, S. J.; Rosi, N. L. High and Selective Co₂ Uptake in a Cobalt Adeninate Metal-Organic Framework Exhibiting Pyrimidine-and Amino-Decorated Pores. *J. Am. Chem. Soc.* **2009**, *132* (1), 38-39.
- (59) Hao, G. P.; Li, W. C.; Qian, D.; Lu, A. H. Rapid Synthesis of Nitrogen-Doped Porous Carbon Monolith for Co₂ Capture. *Adv. Mater.* **2010**, *22* (7), 853-857.
- (60) Silvestre-Albero, J.; Wahby, A.; Sepúlveda-Escribano, A.; Martínez-Escandell, M.; Kaneko, K.; Rodríguez-Reinoso, F. Ultrahigh Co₂ Adsorption Capacity on Carbon Molecular Sieves at Room Temperature. *Chem. Commun.* **2011,** *47* (24), 6840-6842.
- (61) Sevilla, M.; Valle Vigón, P.; Fuertes, A. B. N-Doped Polypyrrole-Based Porous Carbons for Co₂ Capture. *Adv. Funct. Mater.* **2011**, *21* (14), 2781-2787.
- (62) Wickramaratne, N. P.; Jaroniec, M. Importance of Small Micropores in Co₂ Capture by Phenolic Resin-Based Activated Carbon Spheres. *J. Mater. Chem. A* **2013**, *1* (1), 112-116.
- (63) Zhang, J.; Dai, L. Heteroatom-Doped Graphitic Carbon Catalysts for Efficient Electrocatalysis of Oxygen Reduction Reaction. *ACS Catalysis* **2015**, *5* (12), 7244-7253.
- (64) Guo, D.; Shibuya, R.; Akiba, C.; Saji, S.; Kondo, T.; Nakamura, J. Active Sites of Nitrogen-Doped Carbon Materials for Oxygen Reduction Reaction Clarified Using Model Catalysts. *Science* **2016**, *351* (6271), 361-365.
- (65) Conway, B. E. *Electrochemical Supercapacitors: Scientific Fundamentals and Technological Applications*, Springer Science & Business Media: 2013.
- (66) Tanaka, S.; Nakao, H.; Mukai, T.; Katayama, Y.; Miyake, Y. An Experimental Investigation of the Ion Storage/Transfer Behavior in an Electrical Double-Layer Capacitor by Using Monodisperse Carbon Spheres with Microporous Structure. *J. Phys. Chem. C* **2012**, *116* (51), 26791-26799.

(67) Miao, F.; Shao, C.; Li, X.; Wang, K.; Lu, N.; Liu, Y. Three-Dimensional Freestanding Hierarchically Porous Carbon Materials as Binder-Free Electrodes for Supercapacitors: High Capacitive Property and Long-Term Cycling Stability. *J. Mater. Chem. A* **2016**, *4* (15), 5623-5631.

Insert Table of Contents artwork here

